Published in final edited form as:
Liq Cryst. 2013 January 1; 40(12): 1748–1758. doi:10.1080/02678292.2013.846422.

Liquid crystal assemblies in biologically inspired systems

Cyrus R. Safinya[a,*], **Joanna Deek**[a,b,d], **Roy Beck**[a,e], **Jayna B. Jones**[a], **Cecilia Leal**[a,f], **Kai K. Ewert**[a], and **Youli Li**[c]

[a]Materials, Physics, and Molecular, Cellular, & Developmental Biology Departments, University of California, Santa Barbara, CA 93106, USA

[b]Chemistry and Biochemistry Department, University of California, Santa Barbara, CA 93106, USA

[c]Materials Research Laboratory, University of California, Santa Barbara, CA 93106, USA

Abstract

In this paper, which is part of a collection in honor of Noel Clark's remarkable career on liquid crystal and soft matter research, we present examples of biologically inspired systems, which form liquid crystal (LC) phases with their LC nature impacting biological function in cells or being important in biomedical applications. One area focuses on understanding network and bundle formation of cytoskeletal polyampholytes (filamentous-actin, microtubules, and neurofilaments). Here, we describe studies on neurofilaments (NFs), the intermediate filaments of neurons, which form open network nematic liquid crystal hydrogels in axons. Synchrotron small-angle-x-ray scattering studies of NF-protein dilution experiments and NF hydrogels subjected to osmotic stress show that neurofilament networks are stabilized by competing long-range repulsion and attractions mediated by the neurofilament's polyampholytic sidearms. The attractions are present both at very large interfilament spacings, in the *weak sidearm-interpenetrating regime*, and at smaller interfilament spacings, in the *strong sidearm-interpenetrating regime*. A second series of experiments will describe the structure and properties of cationic liposomes (CLs) complexed with nucleic acids (NAs). CL-NA complexes form liquid crystalline phases, which interact in a structure-dependent manner with cellular membranes enabling the design of complexes for efficient delivery of nucleic acid (DNA, RNA) in therapeutic applications.

Keywords

Neurofilaments; nematic hydrogels; lipids; DNA; RNA; lamellar liquid crystals; hexagonal liquid crystals; gyroid cubic phases; small-angle-x-ray-scattering (SAXS)

1. Introduction

The experiments described in this invited paper were designed in order to enable a fundamental understanding of (i) the interactions in filamentous protein assemblies in charged systems and (ii) the structures of cationic liposome-nucleic acid complexes. The in vitro studies of filamentous protein assembly are inspired by the formation of structures, both relatively static and highly dynamic, observed in the cell cytoskeleton, in particular, the cytoskeleton of axons and dendrites [1-7]. Recent studies have focused on understanding

[*]Corresponding author. safinya@mrl.ucsb.edu.
[d]Current address: Lehrstuhl für Zellbiophysik E27, Technische Universität München, Garching, Germany
[e]Current address: Department of Condensed Matter Physics, School of Physics and Astronomy, Tel-Aviv University, 69978 Tel Aviv, Israel
[f]Current address: Materials Science & Engineering Department, University of Illinois at Urbana-Champaign, Urbana, IL 61801, USA

network and bundle formation of biological polyampholytes (containing both positive and negative charge residues) including filamentous actin, [8-16] microtubules, [17-21] and neurofilaments. [22-27] These three filamentous proteins constitute the major protein fraction in the cytoskeleton of neurons. Their persistence lengths range from very large of order millimeters for rigid microtubules to about one micron for semi-flexible filamentous actin and to around 100 nm to 150 nm for flexible neurofilaments. As we describe below this large difference in the biopolymer rigidity leads to quite different hierarchical self-assembled structures for these different filamentous systems.

In studies on microtubules (MTs), 25 nm scale overall negatively charged rigid nanotubes, experiments show that the charge of the counterion modulates the forces between MTs. [17] Unexpectedly the studies reveal a transition from finite-sized 3D bundles (for counterion charge 3+ to 5+) to sheet-like 2D bundles with divalent counterions (see schematic in Fig. 1). Current theories of bundling do not predict the transition from 3D to 2D bundles for like-charged polyelectrolyte rods in the presence of counterions, and the discrepancy between experiment and theory is an area, which remains to be better understood. [28-31] The 3D bundles of MTs, with in-plane hexagonal symmetry observed in small-angle-x-ray-scattering (SAXS) studies, are reminiscent of freely suspended columnar phases of discotic liquid crystals studied by Noel Clark and collaborators in the early 1980s. [32, 33]

One series of experiments, which we describe (in section 2.) will be on studies of phase behavior and interfilament interactions in neurofilament networks, which under physiological conditions tend to form highly oriented nematic liquid crystal (LC) hydrogels. [22, 23, 25, 27] (Neurofilaments are a class of intermediate filaments expressed in vertebrate neurons.) Aside from the importance of understanding the phase behavior of filamentous proteins derived from the cell cytoskeleton both under equilibrium and out-of-equilibrium conditions (e.g. in assembling buffers containing GTP or ATP), such studies will also contribute to our understanding of polyelectrolyte physics, an important subfield of soft condensed matter, where much remains to be understood.

A separate series of experiments will be described (in section 3.), which are centered on studies of cationic liposome-nucleic acid complexes, which spontaneously self-assemble to form highly organized liquid crystalline phases of matter. [34-37] These nanometer scale LC complexes have emerged as favored carriers of exogenous nucleic acids into cells both in studies designed to understand the function of a specific sequence of nucleic acid (e.g. a promoter sequence controlling gene transcription) and also in ongoing human gene therapy clinical trials. [38]

2. Reconstituted neurofilaments: nematic liquid crystal hydrogels

Figure 2 displays an electron micrograph by Nobutaka Hirokawa showing a side view of the cytoskeleton of the axon of a mouse neuron. [7] A vesicle may be seen attached via motors to a single microtubule (MT, red arrow). The motors, in this case Kinesin, are transporting the vesicle and its cargo (e.g. neurotransmitter precursor molecules) in order to deposit the contents at a terminal synapse and enable nerve cell communication. We see in the image that the MT is surrounded by a dense network of neurofilaments (NFs, red stars), which play a major role in the structural stability of the axon. The micrograph also shows that neighboring NFs appear to interact through their protruding sidearms. The sidearm interactions between NFs in axons results in a well-defined average spacing between the oriented NFs (Fig. 2, red star regions). From the micrograph it is clear that the sidearm interactions are non-covalent because they have to locally “unzip and re-zip” as organelles, with much large sizes compared to the NF-network mesh size, move through the network.

Nevertheless, we still do not have a full understanding of the precise nature of the sidearm interactions, which, in turn, impact the axon cytoskeleton stability.

Neurofilaments consist of three different molecular weight polypeptide subunits (Fig. 3 (a), labeled NF-L (L = Low (or Light, 60 kDa); NF-M (M = Medium, 100 kDa); and NF-H (H = High (or Heavy, 115 kDa)). Among the fractions only NF-L will assemble in the absence of the other subunits and form stable filaments. The NF-M or NF-H subunits require the presence of NF-L to form filaments. Purified NF subunits tend to spontaneously assemble to form a 10 nm thick filamentous protein with highly charged C-terminal sidearms, which extend away from the filament [39-41]. An electron micrograph by Aebi et al. [6] of an isolated mature neurofilament clearly displaying protruding flexible sidearms can be seen in Fig. 3 (b) together with a schematic sketch in Fig. 3 (c). For clarity the schematic shows only one short NF-L C-terminal sidearm, which in the real system is the largest mole fraction in heteropolymer NFs with mixed C-terminal sidearms. In buffer mimicking physiological conditions, purified and re-assembled NFs may form an Onsager-like nematic liquid crystal (LC) gel phase (labeled N_G). This is seen in polarized microscopy images in Fig. 3 (d) where the texture is characteristic of a nematic hydrogel with long-range orientational order associated with the filamentous network. [22-27] The neurofilament nematic gel phase, reconstituted in vitro, is a thermodynamically stable phase and at high salt concentrations of order 150 mM (i.e. where the small Debye length ≈ 7.84 Å provides efficient screening) the orientational ordering is due to an Onsager type ordering. Recent experiments confirm the thermodynamic stability of this phase where as a function of decreasing salt concentrations the nematic gel phase undergoes reversible transitions to an isotropic gel followed by a new re-entrant liquid crystal gel phase. [27]

The NF C-terminal sidearms are intrinsically disordered polyampholytes (i.e. containing both positive and negative charge) and network formation is mediated through interactions between the unstructured sidearms (although the precise nature of the interactions is not fully understood). [42, 43, 23, 25-27] In neurons the composition of the three NF subunits is regulated over a narrow range (e.g., in mouse the mole fractions are approximately 7:3:2 for NF-L:NF-M:NF-H) with incorrect compositions resulting in the disruption of the NF-network and motor neuron diseases. [44, 45]

2.1 SAXS and phase behavior in neurofilament liquid crystal hydrogels reveal competing interfilament repulsions and attractions in the weakly sidearm-interpenetrating regime at large interfilament spacings

The phase diagram of reconstituted neurofilaments in buffer may be mapped out using polarized and bright field microscopy. [23, 27] For NF-LM neurofilaments (comprised of NF-L and NF-M subunits) reconstituted at increasing NF-M/NF-L ratios in buffer containing 86 mM NaCl, the samples are in the N_G phase at high wt% total protein. [23] The gel behavior is seen under bright field optical microscopy with the presence of asymmetric interfaces, which indicate that the network has elasticity and resists flow. As the NF-LM gels are diluted in the N_G phase to low wt% total protein, the nematic gel swells until a dilution limit is reached, beyond which a transition to a two-phase nematic gel and isotropic sol (I_s) phase is observed. This transition is around 1.3 ± 0.2 wt% protein for the NF-L homopolymer but increases with the addition of NF-M sidearms to $\approx 2.3 \pm 0.2$ wt% protein at NF-L/NF-M = 65/35 (wt/wt). [23] This composition-dependence of the onset of two-phase behavior is an indication that attractive interfilament interactions are more important at high NF-M sidearm grafting densities and begin preventing hydrogel swelling earlier along the dilution lines at increasingly larger protein concentrations. In contrast, for NF-LH neurofilaments (comprised of NF-L and NF-H subunits) reconstituted ay increasing NF-H/NF-L ratios in buffer containing 86 mM NaCl, polarized microscopy shows that for grafting densities larger than 10 wt% the NF-H sidearms de-stabilize the N_G phase upon dilution for

protein concentrations less than 1.5 +/− 0.2 wt% leading to the isotropic gel phase with randomly oriented filaments coexisting with the sol phase. [23]

Quantitative synchrotron small-angle-x-ray scattering (SAXS) data along protein dilution lines in reconstituted NF mixtures indicate that the sidearms play an essential role in controlling the interfilament interactions at interfilament distances much larger than the filament thickness. [23] We show in Fig. 4 SAXS data of NF-LM and NF-LH neurofilaments assembled in buffer containing 86 mM NaCl. The SAXS profiles enable a measurement of the average spacing (d) between neurofilaments from the position of the maximum in the correlation peak $q = 2\pi/d$ (Fig. 4). At the intermediate NF-M grafting density of NF-L/NF-M = 85/15 (wt/wt) the peak position of the SAXS profiles (Fig. 4, Left) are seen to shift to lower q values as the N_G phase is diluted with decreasing protein concentration. The 3.3 wt% and 2.6 wt% samples are in the 1-phase N_G region and the 1.8 wt% and 1.1 wt% samples are just above and well below the transition boundary to the 2-phase (N_G plus I_s) region, respectively. Over the dilution range in the one-phase N_G phase, we see that the interfilament spacing increases from d = 41.9 +/− 2 nm at 3.3 wt% to d = 52.3 +/− 2 nm at 2.6 wt% and finally to d = 62.9 +/− 4 nm at 1.8 wt% (near the maximum swelling limit). In the 2-phase region at 1.1 wt% the maximum swelling limit (with excess buffer expelled from the NF gel) is at d = 69.8 +/− 4 nm. In contrast, at a high grafting density of NF-L/NF-M = 65/35 (wt/wt) the SAXS peak position from NF-LM filaments is nearly fixed (Fig. 4, Middle), varying only slightly between d = 44 nm and d = 48 nm, over the same range of protein concentrations with no gel swelling below protein concentrations $\approx$ 2.3 +/− 0.2 wt% (the 1.7 wt% and 1.0 wt% samples are in the 2-phase N_G plus I_s region). This limiting spacing in samples with expelled excess buffer is an unambiguous indication of interfilament attractions at large spacings, which are much larger than the filament diameter.

SAXS data for NF-LH gels reveal qualitatively different behavior for interfilament interactions when NF-M sidearms are replaced by NF-H sidearms. [23] Fig. 4 (Right) shows that, upon dilution of the N_G gel phase, for the intermediate NF-H grafting density of NF-L/NF-H = 80/20 (wt/wt), the correlation peak in the SAXS data shifts to lower q ranging from 0.17 $Å^{-1}$ (d = 36.9 +/− 2 nm) to 0.115 $Å^{-1}$ (d = 54.6 +/− 2 nm) in going from the 4.3 wt % to the 2.6 wt % sample. The peak is seen to be absent for the 1.9 wt% sample, while polarized microscopy shows the sample to be in the N_G phase. This indicates that the filaments are still moving further apart upon dilution but that filament undulations are broadening and weakening the peak. Along this dilution line the 1.5 wt % sample is a typical example in the isotropic gel (I_G) plus sol (I_S) 2-phase region, which shows enhanced SAXS but no clear correlation peak. The lack of a clear SAXS correlation peak, even in the 1-phase region just above the N_G to I_G transition, means that cryogenic TEM (which does not distort structure and would yield accurate interfilament spacings) would be required to characterize the dilution behavior of NF-LH gels in this very dilute regime. Similar behavior is observed along other NF-LH dilution lines with increasing NF-H up to NF-L/NF-H = 70/30 (wt/wt). [23] Thus, in contrast to the behavior observed for NF-LM filaments in excess buffer, where a high NF-M sidearm grafting density leads to strongly attractive nematic gels in buffers containing 86 mM NaCl, NF-LH hydrogels in the same buffer, with NF-H sidearm composition larger than 10 wt%, results in sufficiently large repulsive interfilament interactions to destabilize and transform the nematic gel to an isotropic gel phase. The transition should be expected to occur when the interfilament spacing becomes either of the order of the persistence length of NFs or the contour length of the purified and reconstituted filaments $\approx$ 200 nm. [26] Cryo-TEM studies of the interfilament spacings in the transition regime would clarify the origin of the N_G to I_G transtions.

The observed maximum swelling limit for NF-LM nematic hydrogels in excess buffer is a reflection of a competition between repulsive interactions, which dominate in the 1-phase (N_G) region, and attractive interfilament interactions, which are dominant in the 2-phase ($N_G + I_s$) region. Furthermore, the SAXS data For NF-LM nematic gels (Fig. 4, Left and Middle), show that the optimal equilibrium spacing in excess buffer decreases from d ≈ 69.8 +/− 4 nm for (NF-L/NF-M = 85/15, wt/wt) to d ≈ 46 +/− 2 nm for (NF-L/NF-M = 65/35, wt/wt) reflective of the enhanced interfilament attractions with increased NF-M grafting density. The origin of the repulsions is screened electrostatic interactions of the flexible and undulating NF-filaments. [46-49] Because the van der Waals attraction [50] is expected to be negligible at these large spacings (i.e. where the wall-to-wall spacing between filament rods is ≈ 3.6 +/− 0.2 nm), we conclude that the attractions most likely originate in the interactions between NF-M sidearms; in particular, between anionic/cationic groups of apposing sidearms brought into contact due to the neurofilament backbone undulations. These attractions, in the *weak sidearm-interpenetrating regime at large spacings*, compete with and balance the repulsive electrostatic interactions between filaments. [23]

2.2 SAXS-osmotic pressure experiments reveal the presence of short-range attractions between interpenetrating sidearms in neurofilament liquid crystal hydrogels

Aside from the observed attractions at large interfilament spacings, force measurements of neurofilament hydrogels, subjected to osmotic pressure, have revealed the existence of attractions at much shorter spacings. [25] With increasing pressure near physiological salt conditions (150 mM, 240 mM) NF-LH gels, comprised of NF-L and NF-H subunits, have been observed to undergo, above a critical pressure $P > P_c \approx 10^4$ Pa, an abrupt non-reversible transition from an expanded-network to a condensed-network with strong sidearm interpenetration (Fig. 5a). In contrast, NF-LM gels remain in a collapsed state for $P < P_c$ and only for low ionic strengths (40 mM, 70 mM) show an expanded isotropic gel phase at $P < P_c$ and the transition to the condensed-network state at $P > P_c$ (Fig. 5b). Interestingly, the NF-LMH network, comprised of the three subunits with near in vivo axon compositions (7:3:2 molar ratio for NF-L:NF-M:NF-H), exhibits the same expanded-network to condensed-network transition observed in NF-LH hydrogels (Fig. 5c).

The expanded-network to condensed-network transition, seen in SAXS as an abrupt decrease in interfilament spacing over a small pressure range near P_c, is a clear signature of the onset of attractions between anionic and cationic residues in the *strong sidearm-interpenetrating regime* overwhelming the longer ranged electrostatic repulsions between neurofilaments. This observed behavior is consistent with an electrostatic calculation of interpenetrating polyampholyte chains with short-range attractions between oppositely charged amino acid residues on neighboring sidearms. [25] Thus, the SAXS-osmotic pressure technique allows one to quantitatively probe inter-filament forces in NF hydrogels, in particular, the onset of attractions, and differentiate between distinct roles of NF-M and NF-H sidearms in regulating inter-filament interactions and spacings, both at very low and high osmotic pressures mimicking the crowded environment in neuronal processes.

3. Cationic liposome-nucleic acid complexes: liquid crystals with medical applications

The discovery of liposomes (spherical lipid assemblies) by A. D. Bangham during the early 1960s was a landmark event, which precipitated intense interest in the scientific community. [51] Because of their similarities to biological membranes, they are used in model studies of cell-cell interactions. Furthermore, their encapsulation properties led rapidly to their use as chemical carriers and liposomes will continue to have a major impact in the medical field as

drug and gene carriers. [52] In more recent times cationic liposomes (CLs) have emerged as highly prevalent carriers for transferring nucleic acid (DNA, RNA) into cells for gene therapy and medical therapeutics. [53-56] Currently over one hundred clinical trials are ongoing worldwide, which utilize cationic liposomes as the gene carrier to address a range of medical conditions from cystic fibrosis to cancer. [38, 57]

Viral-based methods of gene delivery are important and efficient but they also have, on occasion, led to undesirable severe immune responses and cancers in patients. [58-60] Synthetic carriers (or vectors) are of interest because of their ease of use, their non-immunogenicity in comparison to viral vectors, and the potential of transferring large pieces of DNA, including entire genes (containing coding and noncoding domains) and regulatory sequences, into cells. [61, 62] In contrast viral capsids limit the transfer of genes to complementary DNA (i.e. DNA synthesized from mRNA, which excludes noncoding introns). However, transfection efficiency (TE, a measure of the ability of the carrier to deliver an exogenous gene followed by expression) remains low compared to viral vectors and only a significant further increase in our knowledge of the interactions between CL-DNA complexes and cells will result in optimization of TE. [54-56] Indeed determining the precise structural nature of CL-DNA complexes [34-37, 63] is crucial because it will naturally lead to a better understanding of the interactions between complexes and cellular membranes. [64, 65]

Studies using synchrotron x-ray scattering have led to the discovery of four distinct structures observed in CL-DNA complexes. [34-36, 66] The first two structures described are shown schematically in Fig. 6 (Top) and include a multilamellar phase with DNA layers sandwiched between cationic bilayer membranes (L_α^C), [34] and an inverted hexagonal structure with DNA encapsulated within cationic lipid monolayer tubes (H_{II}^C). [35] The lamellar CL-DNA complex may be viewed as a “hybrid” phase of matter, namely, a 2D smectic phase of DNA chains coupled to lipid bilayers, which form a 3D smectic phase. On large enough length scales (which has not been achieved experimentally) the 2D smectic lattice is expected to melt into a 2D nematic phase of DNA chains due to dislocations. [67-69]

One may understand the shapes assumed by the membranes of CL-DNA complexes by considering the Helfrich elastic curvature energy of lipid membranes per unit area $F/A = 0.5\ \kappa\ (C - C_o)^2 + \kappa_G\ C_1C_2$ [70-72]. Here, $C = C_1 + C_2$ is the mean curvature and C_1C_2 the Gaussian curvature, with $C_1 = 1/R_1$ and $C_2 = 1/R_2$ the curvatures along the “1” and “2” axes (with R_1, R_2 the membrane radii), C_o the spontaneous curvature, and κ and κ_G the membrane bending and Gaussian moduli, respectively. The “shape” of the lipid molecule, in its local membrane environment, determines the spontaneous curvature of the membrane C_o.[50, 70-72]

The first term in the elastic energy measures the cost of curvature deviations away from C_o. Thus, for large enough κ compared to thermal energies, lipids with a cylindrical shape such as 1,2-dioleoyl-*sn*-glycero-3-phosphocholine (DOPC), with head group area approximately equal to the tail area ($C_o = 0$), tend to assemble into lamellar lipid-bilayer structures with $C = 0$ in order to minimize elastic costs. Similarly lipids with an inverse cone shape like 1,2-dioleoyl-*sn*-glycero-3-phosphoethanolamine (DOPE), with head group area less than the tail area ($C_o < 0$), tend to assemble into inverse micellar structures with $C < 0$. For example, the first lamellar L_α^C phase to be described consisted of a lipid mixture of cationic 1,2-dioleoyl-3-trimethylammonium-propane (chloride salt) (DOTAP) mixed with neutral DOPC, and both lipids have a cylindrical shape (i.e. $C_o = 0$). [34] Similarly, the initial studies of inverse hexagonal H_{II}^C phases consisted of cationic liposomes of DOTAP and

DOPE (with weight fraction of DOPE between 0.7 and 0.85) where the membrane mixture has a negative spontaneous curvature $C_o < 0$. [35]

The Helfrich elastic energy also predicts that cone shaped lipids with head group area larger than tail area ($C_o > 0$) usually assemble into spheroidal or rod-like micellar structures with $C > 0$. Indeed, experiments show that when DNA is complexed with mixtures of DOPC and custom synthesized lipid MVLBG2, a highly charged (16^+) multivalent cationic lipid, a novel hexagonal complex is stabilized in a narrow range of composition ≈ 25 mol % MVLBG2. [36] In this novel dual lattice structure, termed H_I^C, hexagonally arranged rod-shaped lipid micelles (with $C > 0$) are surrounded by DNA, which, in turn, form a continuous substructure with honeycomb symmetry (Fig. 6 Bottom right).

The Gaussian curvature term in the Helfrich elastic curvature energy implies that in addition to the shapes described above (sheets and cylinders), which have $C_1C_2 = 0$, lipids with a positive Gaussian modulus $\kappa_G > 0$ will tend to form saddle-splay shaped membranes with negative Gaussian curvature $C_1C_2 < 0$. [70-74] (This is in contrast to lipids with $\kappa_G < 0$, which prefer to form spheres with positive $C_1C_2 > 0$.) Examples are lipid-water systems forming bicontinuous cubic phases. [73, 74] As we describe below novel cationic Gyroid cubic phases complexed with short RNA molecules have been recently described. [37, 75]

Before leaving this section we should point out that comprehensive theoretical treatments on the thermodynamic stability of CL-DNA complexes, which, in addition to the membrane elasticity, incorporate the electrostatic effects between oppositely charged membranes and anionic DNA, have been carried out [76-79] and are consistent with experiments. The experimental discovery of the novel lamellar phase of lipid-DNA complexes motivated theoretical discoveries by Tom Lubensky and C. O'Hern and independently Leo Golubovic and M. Golubovic on the possible existence of entirely new “sliding phases” of matter with the ground state consisting of a mixed columnar-lamellar phase in which the lipid forms a regular smectic phase and the DNA forms a periodic aligned columnar lattice with a periodic row sandwiched between pairs of lipid bilayers. [67-69] At higher temperatures positional coherence between DNA columns in adjacent layers could be lost but without destroying orientational coherence of DNA columns between layers. Or both positional and orientational coherence between layers could be lost. Theory indicates that the orientationally ordered but positionally disordered “sliding” phase can exist and that there can be a phase transition between it and the columnar phase. This remarkable phase of matter remains to be discovered in the laboratory.

3.1 Cationic liposome/short-interfering-RNA complexes in gene silencing

The discovery of RNA interference (RNAi) as a post-transcriptional gene silencing pathway has recently led to research on cationic liposome nucleic acid complexes in order to silence aberrant genes. The finding that short strands of dsRNA (21-25 bp, with 2-nucleotide 3′-overhangs) termed siRNA enabled sequence specific gene silencing in mammalian cells has led to numerous research groups utilizing the pathway more broadly in studies of functional genomics. [80-85] Cationic liposomes offer the potential to deliver siRNA for both functional genomics and therapeutic silencing of aberrant genes. [86, 87]

Recent studies reported on the development of a novel double gyroid cationic lipid cubic phase, which incorporates short functional siRNA molecules within its two water channels (Fig. 7, Left). Synchrotron SAXS data displayed in Fig. 7 (Right) has confirmed the inverse bicontinuous cubic structure for these CL-siRNA complexes. [37]

The significance of the gyroid cubic phase is that the lipids of the bicontinuous structure with $C_1C_2 < 0$, when brought into contact with apposing membranes, are expected to rapidly

fuse because such a process leads to the formation of membrane pores, which also have negative Gaussian curvature interfaces. The results of the study are consistent with the hypothesis that the cubic phase-siRNA complex, upon cell entry via endocytosis, escapes the endosome by punching holes in the surrounding membrane leading to efficient cytoplasmic delivery of siRNA and sequence-specific gene silencing. [37]

4. Concluding remarks

Liquid crystal and soft condensed matter physics have had and will continue to have a large impact on our understanding of interactions, phases, and distinct structures in biologically related systems. For neurofilament networks it is becoming more clear that while the precise nature of the non-covalent NF sidearm-sidearm interactions remains to be fully understood, short-range electrostatic attractions between the opposite charges on the polyampholyte sidearms, appear to be important. This is true not only in the regime where the sidearms are forced to interpenetrate, but also in the weakly interpenetrating regime, in the absence of osmotic pressure, where the undulating neurofilament backbone allows for close approach of neighboring sidearms. We note that the attractions resulting from the interaction between protruding intrinsically disordered NF-sidearms is a property of polyampholytes, not present (in the absence of multivalent counterions) for those polyelectrolytes where the charged units are either all positive or all negative.

As mentioned earlier one significant reason cationic liposome-nucleic acid complexes are studied worldwide is because they are currently being employed in human clinical trials. In an effort to develop an understanding of the chemical-physical parameters that control transfection by cationic liposome carriers, transfection efficiency studies with complexes with distinct structures are currently being carried out in numerous laboratories worldwide. Indeed, intensive research in the last two decades has led to nonviral vectors, which are fully competitive with engineered viral vectors *for in vitro applications*. For example, multivalent lipid MVL5 (5+) synthesized [88] and characterized [65, 87] in our laboratory at Santa Barbara has been recently commercialized and is currently marketed by Avanti Lipids, Inc. [89]. When formulated as lamellar liquid crystal MVL5-siRNA nanoparticles, MVL5 may be used in gene silencing applications (either for therapeutics or functional genomics studies) with improved properties, including total gene silencing, lower non-specific gene silencing, and lower toxicity, in comparison to standard commercial lipid transfection reagents such as Lipofectamine 2000. The challenge for the future remains in developing efficient nonviral vectors for in vivo applications (e.g. in blood) an area where engineered viral vectors are far superior. Of course viral technology presents other challenges, in particular, the possibility of severe immune reactions. In the final analysis, it appears almost certain that, in addition to in vivo studies, developing efficient carriers of nucleic acids will require further more comprehensive in vitro studies; for example, through live cell imaging, which enable spatial-temporal mapping of intracellular complex pathways and their interactions with cellular components.

Acknowledgments

CRS, JD, KKE, and YL acknowledge support by the U.S. Department of Energy-Basic Energy Sciences grant number DOE-DE-FG02-06ER46314 (self-assembly and interactions in filamentous protein systems), the U.S. National Institutes of Health GM-59288 (biological activity studies in cationic liposome-DNA complexes), and the U.S. National Science Foundation DMR-1101900 (protein phase behavior). CL was funded by the Swedish Research Council (VR) and in part by the US DOE-BES. RB was supported by the Human Frontier Science Program organization, the Israeli Science Foundation (Individual Research Grant 571/11), the European Community's 7th Framework Programme (293402), and the Sackler Institute for Biophysics at Tel-Aviv University. The X-ray diffraction work was carried out at the Stanford Synchrotron Radiation Laboratory (SSRL) beam lines 7.2 and 4.2. CRS acknowledges useful discussions with KAIST Faculty where he has a WCU (World Class

University) Visiting Professor of Physics appointment supported by the National Research Foundation of Korea funded by the Ministry of Education, Science and Technology No. R33-2008-000-10163-0.

References

1. Kandel, ER.; Schwartz, JH.; Jessell, TM. Principles of Neural Science. 4th. McGraw Hill; New York: 2000.
2. Peters, A.; Palay, SL.; Def, H. The Fine Structure of the Nervous System. 3rd. Webster; New York: 1991.
3. Burgoyne, RD., editor. The Neuronal cytoskeleton. Wiley & Sons; New York: 1991.
4. Hirokawa, N. The Neuronal Cytoskeleton. Burgoyne, RD., editor. Wiley; New York: 1991. p. 5-74.
5. Hirokawa N. Cross-linker system between neurofilaments, microtubules and membranous organelles in frog axons revealed by the quick-freeze, deep-etching method. J Cell Biol. 1982; 94:129–142. [PubMed: 6181077]
6. Herrmann, H.; Kreplak, L.; Aebi, U. Methods in Cell Biology. Omary, MB.; Pierre, AC., editors. Vol. 78. Academic Press; Waltham, MA: 2004. p. 3-24.
7. Hirokawa N. Organelle transport along microtubules - the role of KIFs. Trends Cell Biol. 1996; 6:135–141. [PubMed: 15157476]
8. Safinya, CR. Biophysics and Biomaterials, in The New Physics for the Twenty First Century. Fraser, G., editor. Cambridge University Press; Cambridge: 2006.
9. Wong GCL, Lin A, Tang JX, Li Y, Janmey PA, Safinya CR. Lamellar phase of stacked two-dimensional rafts of actin filaments. Phys Rev Lett. 2003; 91:018103. [PubMed: 12906579]
10. Pelletier O, Pokidysheva E, Hirst LS, Bouxsein N, Li Y, Safinya CR. Structure of actin cross-linked with alpha-actinin: A network of bundles. Phys Rev Lett. 2003; 91:148102. [PubMed: 14611558]
11. Hirst LS, Safinya CR. Phys. Skin layer at the actin-gel surface: Quenched protein membranes form flat, crumpled, and tubular morphologies. Phys Rev Lett. 2004; 93:018101. [PubMed: 15324022]
12. Hirst LS, Pynn R, Bruinsma RF, Safinya CR. Hierarchical self-assembly of actin bundle networks: Gels with surface protein skin layers. J Chem Phys. 2005; 123:104902. [PubMed: 16178619]
13. Ikawa T, Hoshino F, Watanabe O, Li YL, Pincus P, Safinya CR. Molecular scale imaging of F-actin assemblies immobilized on a photopolymer surface. Phys Rev Lett. 2007; 98:018101. [PubMed: 17358507]
14. Angelini TE, Liang H, Wriggers W, Wong GCL. Like-charge attraction between polyelectrolytes mediated by counterion charge density waves. Proc Natl Acad Sci USA. 2003; 100:8634. [PubMed: 12853566]
15. Wong GCL. Electrostatics of rigid polyelectrolyte. Curr Opin Colloid Interface Sci. 2006; 11:310.
16. Wong GCL, Pollack L. Electrostatics of Strongly Charged Biological Polymers: Ion-Mediated Interactions and Self-Organization in Nucleic Acids and Proteins. Annu Rev Phys Chem. 2010; 61:171. [PubMed: 20055668]
17. Needleman DJ, Ojeda-Lopez MA, Raviv U, Miller HP, Wilson L, Safinya CR. Higher-order assembly of microtubules by counterions: From hexagonal bundles to living necklaces. Proc Natl Acad Sci USA. 2004; 101:16099–16103. [PubMed: 15534220]
18. Choi MC, Raviv U, Miller HP, Gaylord MR, Kiris E, Ventimiglia D, Needleman DJ, Kim MW, Wilson L, Feinstein SC, Safinya CR. Human Microtubule-Associated-Protein Tau Regulates the Number of Protofilaments in Microtubules: A Synchrotron X-ray Scattering Study. Biophys J. 2009; 97:519–527. [PubMed: 19619466]
19. Safinya CR, Raviv U, Needleman DJ, Zidovska A, Choi MC, Ojeda-Lopez MA, Ewert KK, Li Y, Miller HP, Quispe J, Carragher B, Potter CS, Kim MW, Feinstein SC, Wilson L. Nanoscale Assembly in Biological Systems: From Neuronal Cytoskeletal Proteins to Curvature Stabilizing Lipids. Adv Mater. 2011; 23:2260–2270. [PubMed: 21506171]
20. Needleman DJ, Ojeda-Lopez MA, Raviv U, Miller HP, Li Y, Song C, Feinstein SC, Wilson L, Choi MC, Safinya CR. Faraday Discussions. 166 in press. 10.1039/C3FD00063J
21. Ojeda-Lopez MA, Needleman DJ, Song C, Ginsburg A, Kohl PA, Li Y, Miller HP, Wilson L, Raviv U, Choi MC, Safinya CR. Molecularly-triggered conformation switch in tubulin in taxol-

stabilized microtubules leads to bundles of inverted protein tubules. Nature Materials. under review.

22. Needleman DJ, Jones JB, Raviv U, Ojeda-Lopez MA, Miller HP, Li Y, Wilson L, Safinya CR. Supramolecular assembly of biological molecules purified from bovine nerve cells: from microtubule bundles and necklaces to neurofilament networks. J Phys: Condens Matter. 2005; 17:S3225–S3230.
23. Jones JB, Safinya CR. Interplay between Liquid Crystalline and Isotropic Gels in Self-Assembled Neurofilament Networks. Biophys J. 2008; 95:823–825. [PubMed: 18583309]
24. Hesse HC, Beck R, Ding C, Jones JB, Deek J, MacDonald NC, Li Y, Safinya CR. Direct Imaging of Aligned Neurofilament Networks Assembled Using In Situ Dialysis in Microchannels. Langmuir. 2008; 24:8397–8401. [PubMed: 18336050]
25. Beck R, Deek J, Jones JB, Safinya CR. Gel Expanded–Gel Condensed Transition in Neurofilament Networks Revealed by Direct Force Measurements. Nature Mat. 2010; 9:40–46.
26. Beck R, Deek J, Choi MC, Ikawa T, Watanabe O, Frey E, Pincus PA, Safinya CR. Unconventional Salt-Switch from Soft to Stiff in Single Neurofilament Biopolymers. Langmuir. 2010; 26:18595–18599. [PubMed: 21082794]
27. Deek J, Chung PJ, Kayser J, Bausch AR, Safinya C. Neurofilament sidearms modulate parallel and crossed-filament orientations inducing nematic to isotropic and re-entrant birefringent hydrogels. Nature Communications. 2013; 4:2224.
28. Oosawa F. Interaction between parallel rodlike macroions. Biopolymer. 1968; 6:1633–1639.
29. Manning GS. Limiting Laws and Counterion Condensation in Polyelectrolyte Solutions I. Colligative Properties. J Chem Phys. 1969; 51:924–933.
30. Gronbech-Jensen N, Mashl RJ, Bruinsma RF, Gelbart WM. Counterion-Induced Attraction between Rigid Polyelectrolytes. Phys Rev Lett. 1997; 78:2477–2480.
31. Gelbart WM, Bruinsma RF, Pincus PA, Parsegian VA. DNA-inspired electrostatics. Physics Today. 2000 Sep.53:38–45.
32. Van Winkle DH, Clark NA. Freely Suspended Strands of Tilted Columnar Liquid Crystal Phases: One Dimensional Nematics with Orientational Jumps. Phys Rev Lett. 1982; 48:1407–1410.
33. Safinya CR, Liang KS, Varady WA, Clark NA, Andersson G. Synchroton X-ray Study of the Orientational Ordering D2-D1 Structural Phase Transition of Freely Suspended Discotic Strands in Triphenylene-Hexa-dodecanoate. Phys Rev Lett. 1984; 53:1172–1175.
34. Rädler JO, Koltover I, Salditt T, Safinya CR. Structure of DNA-cationic liposome complexes: DNA intercalation in multilamellar membranes in distinct interhelical packing regimes. Science. 1997; 275:810–814. [PubMed: 9012343]
35. Koltover I, Salditt T, Rädler JO, Safinya CR. An inverted hexagonal phase of cationic liposome-DNA complexes related to DNA release and delivery. Science. 1998; 281:78–81. [PubMed: 9651248]
36. Ewert KK, Evans HM, Zidovska A, Bouxsein NF, Ahmad A, Safinya CR. A columnar phase of dendritic lipid-based cationic liposome-DNA complexes for gene delivery: Hexagonally ordered cylindrical micelles embedded in a DNA honeycomb lattice. J Am Chem Soc. 2006; 128:3998–4006. [PubMed: 16551108]
37. Leal C, Bouxsein NF, Ewert KK, Safinya CR. Highly efficient gene silencing activity of siRNA embedded in a nanostructured gyroid cubic lipid matrix. J Am Chem Soc. 2010; 132:16841–16847. [PubMed: 21028803]
38. Gene Therapy Clinical Trials Worldwide. [accessed June 20, 2013] The journal of gene medicine clinical trial site. 2013. http://www.wiley.com/legacy/wileychi/genmed/clinical/
39. Cohlberg JA, Hajarian H, Tran T, Alipourjeddi P, Noveen A. Neurofilament protein heterotetramers as assembly intermediates. J Biol Chem. 1995; 270:9334–9339. [PubMed: 7721855]
40. Ching G, Liem RJ. Assembly of type IV neuronal intermediate filaments in nonneuronal cells in the absence of preexisting cytoplasmic intermediate filaments. J Cell Biol. 1993; 122:1323–1335. [PubMed: 8376465]
41. Fuchs E, Cleveland DW. A structural scaffolding of intermediate filaments in health and disease. Science. 1998; 279:514–519. [PubMed: 9438837]

42. Hirokawa N, Glicksman MA, Willard MB. Organization of mammalian neurofilament polypeptides within the neuronal cytoskeleton. J Cell Biol. 1984; 98:1523–1536. [PubMed: 6425303]
43. Hoffman PN, Price DL. Neurofilament gene expression: a major determinant of axonal caliber. Proc Natl Acad Sci USA. 1987; 84:3472–3476. [PubMed: 3472217]
44. Miller CCJ, Ackerley S, Brownlees J, Grierson AJ, Jacobsen NJO, Thornhill P. Axonal transport of neurofilaments in normal and disease states. Cell Mol Life Sci. 2002; 59:323–330. [PubMed: 11924605]
45. Janmey PA, Leterrier JF, Herrmann H. Assembly and structure of neurofilaments. Curr Opin Colloid Interface Sci. 2003; 8:40–47.
46. Nelson, DR. Defects and Geometry in Condensed Matter Physics. Cambridge University Press; Cambridge: 2002.
47. Selinger JV, Bruinsma RF. Hexagonal and nematic phases of chains. II. Phase transitions. Phys Rev A. 1993; 43:2922–2931. [PubMed: 9905359]
48. Selinger JV, Bruinsma RF. Hexagonal and nematic phases of chains. I. Correlation functions. Phys Rev A. 1993; 43:2910–2921. [PubMed: 9905358]
49. Roux D, Coulon C. Modelling interactions in microemulsion phases. J Physique. 1986; 47:1257–1264.
50. Israelachvili, JN. Intermolecular and Surface Forces. 2nd. Academic Press; London: 1992.
51. Bangham AD, Horne RW, Bangham AD, Horne RW. NEGATIVE STAINING OF PHOSPHOLIPIDS AND THEIR STRUCTURAL MODIFICATION BY SURFACE-ACTIVE AGENTS AS OBSERVED IN THE ELECTRON MICROSCOPE. J Mol Biol. 1964; 8:660–668. [PubMed: 14187392]
52. Lasic, DD.; Martin, F., editors. Stealth Liposomes. CRC Press, Inc.; Boca Raton: 1995.
53. Felgner PL, Gader TR, Holm M, Roman R, Chan HW, Wenz M, Northrop JP, Ringold GM, Danielsen M. Lipofection: A highly efficient, lipid-mediated DNA-transfection procedure. Proc Natl Acad Sci USA. 1987; 84:7413–7417. [PubMed: 2823261]
54. Bielke, W.; Erbacher, C., editors. Nucleic Acid Transfection. Vol. 296. Springer; Heidelberg: 2010. Topics in Current Chemistry.
55. Huang, L.; Hung, MC.; Wagner, E., editors. Non-Viral Vectors for Gene Therapy. 2nd. Vol. 53. Part I Elsevier; San Diego: 2005. Advances in Genetics.
56. Ewert KK, Zidovska A, Ahmad A, Bouxsein NF, Evans HM, McAllister CS, Samuel CE, Safinya CR. Cationic Lipid–Nucleic Acid Complexes for Gene Delivery and Silencing: Pathways and Mechanisms for Plasmid DNA and siRNA. Topics Curr Chem. 2010; 296:191–226.
57. Nabel GJ, Nabel EG, Yang ZY, Fox BA, Plautz GE, Gao X, Huang L, Shu S, Gordon D, Chang AE. Direct gene transfer with DNA-liposome complexes in melanoma: Expression, biologic activity, and lack of toxicity in humans. Proc Nat Acad Sci USA. 1993; 90:11307–11311. [PubMed: 8248244]
58. Williams DA, Baum C. Medicine. Gene therapy--new challenges ahead. Science. 2003; 302:400–401. [PubMed: 14563994]
59. Thomas CE, Ehrhardt A, Kay MA. Progress and problems with the use of viral vectors for gene therapy. Nature Rev Genet. 2003; 4:346–358. [PubMed: 12728277]
60. Hacein-Bey-Abina S, Garrigue A, Wang GP, Soulier J, Lim A, Morillon E, Clappier E, Caccavelli L, Delabesse E, Beldjord K, Asnafi V, MacIntyre E, Dal Cortivo L, Radford I, Brousse N, Sigaux F, Moshous D, Hauer J, Borkhardt A, Belohradsky BH, Wintergerst U, Velez MC, Leiva L, Sorensen R, Wulffraat N, Blanche S, Bushman FD, Fischer A, Cavazzana-Calvo M. Insertional oncogenesis in 4 patients after retrovirus-mediated gene therapy of SCID-X1. J Clin Invest. 2008; 118:3132–3142. [PubMed: 18688285]
61. Harrington JJ, Van Bokkelen G, Mays RW, Gustashaw K, Willard HF. Formation of de novo centromeres and construction of first-generation human artificial microchromosomes. Nature Genetics. 1997; 15:345–355. [PubMed: 9090378]
62. Roush W. Molecular Biology: Counterfeit Chromosomes for Humans. Science. 1997; 276:38–39. [PubMed: 9122708]

63. Safinya CR. Structures of lipid-DNA complexes: supramolecular assembly and gene delivery. Curr Opin Struct Biol. 2001; 11:440–448. [PubMed: 11495736]
64. Lin AJ, Slack NL, Ahmad A, George CX, Samuel CE, Safinya CR. Three-dimensional imaging of lipid gene-carriers: Membrane charge density controls universal transfection;behavior in lamellar cationic liposome-DNA complexes. Biophys J. 2003; 84:3307–3316. [PubMed: 12719260]
65. Ahmad A, Evans HM, Ewert K, George CX, Samuel CE, Safinya CR. New multivalent cationic lipids reveal bell curve for transfection efficiency versus membrane charge density: lipid-DNA complexes for gene delivery. J Gene Med. 2005; 7:739–748. [PubMed: 15685706]
66. Zidovska A, Evans HM, Ewert KK, Quispe J, Carragher B, Potter CS, Safinya CR. Liquid Crystalline Phases of Dendritic Lipid–DNA Self-Assemblies: Lamellar, Hexagonal and DNA Bundles. J Phys Chem B. 2009; 113:3694–3703. [PubMed: 19673065]
67. O'Hern C, Lubensky T. Sliding columnar phase of DNA lipid complexes. Phys Rev Lett. 1998; 80:4345–4348.
68. Golubović L, Golubović M. Fluctuations of quasi-two-dimensional smectics intercalated between membranes in multi lamellar phases of DNA-cationic lipid complexes. Phys Rev Lett. 1998; 80:4341–4344.
69. Golubović L, Lubensky T, O'Hern C. Structural Properties of the Sliding Columnar Phase in Layered Liquid Crystalline Systems. Phys Rev E. 2000; 62:1069–1094.
70. Helfrich W. Elastic Properties of Lipid Bilayers: Theory and Possible Experiments. Z Naturforsch. 1973; C 28:693–703.
71. Lipowsky, R.; Sackmann, E. Structure and Dynamics of Membranes. Vol. 1A. Elsevier; Amsterdam: 1995.
72. Safran, SA. Statistical Thermodynamics of Surfaces, Interfaces, and Membranes. Addison-Wesley; Reading, MA: 1994.
73. Seddon JM. Structure of the inverted hexagonal (HII) phase, and non-lamellar phase transitions of lipids. Biochim Biophys Acta. 1990 Feb 28; 1031(1):1–69. [PubMed: 2407291]
74. Gruner SM. Stability of Lyotropic Phases with Curved Interfaces. J Phys Chem. 1989; 93:7562–7570.
75. Leal C, Ewert KK, Shirazi RS, Bouxsein NF, Safinya CR. Nanogyroids Incorporating Multivalent Lipids: Enhanced Membrane Charge Density and Pore Forming Ability for Gene Silencing. Langmuir. 2011; 27:7691–7697. [PubMed: 21612245]
76. May S, Ben-Shaul A. DNA-lipid complexes: stability of honeycomb-like and spaghetti-like structures. Biophys J. 1997 Nov; 73(5):2427–2440. [PubMed: 9370436]
77. Bruinsma R. ELECTROSTATICS OF DNA CATIONIC LIPID COMPLEXES - ISOELECTRIC INSTABILITY. Eur Phys J B. 1998; 4:75–88.
78. Bruinsma R, Mashl J. LONG-RANGE ELECTROSTATIC INTERACTION IN DNA CATIONIC LIPID COMPLEXES. Europhys Lett. 1998; 41:165–170.
79. Harries D, May S, Gelbart WM, Ben-Shaul A. Structure, stability, and thermodynamics of lamellar DNA-lipid complexes. Biophys J. 1998 Jul; 75(1):159–173. [PubMed: 9649376]
80. Fire A, Xu SQ, Montgomery MK, Kostas SA, Driver SE, Mello CC. Potent and specific genetic interference by double-stranded RNA in Caenorhabditis elegans. Nature. 1998; 391:806–811. [PubMed: 9486653]
81. Elbashir SM, Harborth J, Lendeckel W, Yalcin A, Weber K, Tuschl T. Duplexes of 21-nucleotide RNAs mediate RNA interference in cultured mammalian cells. Nature. 2001; 411:494–498. [PubMed: 11373684]
82. Cogoni C, Macino G. Post-transcriptional gene silencing across kingdoms. Curr Opin Genet Dev. 2000; 10:638–643. [PubMed: 11088014]
83. Caplen NJ, Parrish S, Imani F, Fire A, Morgan RA. Specific inhibition of gene expression by small double-stranded RNAs in invertebrate and vertebrate systems. Proc Natl Acad Sci USA. 2001; 98:9742–9747. [PubMed: 11481446]
84. Hannon GJ, Rossi JJ. Unlocking the potential of the human genome with RNA interference. Nature. 2004; 431:371–378. [PubMed: 15372045]

85. Karagiannis TC, El-Osta A. RNA interference and potential therapeutic applications of short interfering RNAs. Cancer Gene Ther. 2005; 12:787–795. [PubMed: 15891770]

86. Sioud M. Therapeutic siRNAs. Trends Pharm Sci. 2004; 25:22–28. [PubMed: 14723975]

87. Bouxsein NF, McAllister CS, Ewert KK, Samuel CE, Safinya CR. Structure and gene silencing activities of monovalent and pentavalent cationic lipid vectors complexed with siRNA. Biochemistry. 2007; 46:4785–4792. [PubMed: 17391006]

88. Ewert K, Ahmad A, Evans HM, Schmidt HW, Safinya CR. Efficient synthesis and cell-transfection properties of a new multivalent cationic lipid for nonviral gene delivery. J Med Chem. 2002; 45:5023–5029. [PubMed: 12408712]

89. See e.g. Cationic lipids (Transfection)/multivalent cationic lipid at http://www.avantilipids.com, or http://www.avantilipids.com/index.php?option=com_content&view=article&id=2422&Itemid=616&catnumber=890000

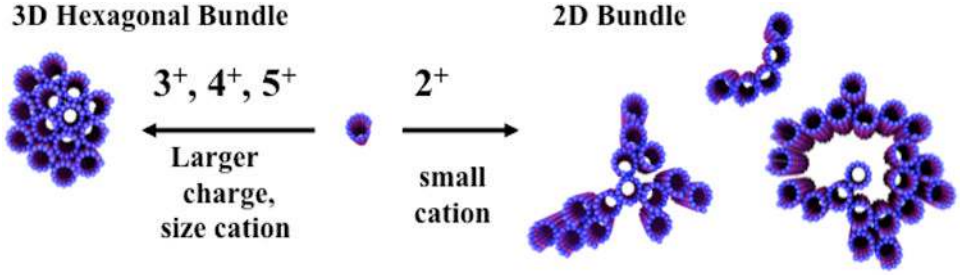

Figure 1.

Schematic of higher-order-assembly of microtubules in the presence of multivalent counterions. (**Left**) Trivalent (spermidine $[H_3N^+\text{-}(CH_2)_3\text{-}^+NH_2\text{-}(CH_2)_4\text{-}^+NH_3]$ and $lysine_3$), tetravalent (spermine $[H_3N^+\text{-}(CH_2)_3\text{-}^+NH_2\text{-}(CH_2)_4\text{-}^+NH_2\text{-}(CH_2)_3\text{-}^+NH_3]$ and $lysine_4$), and pentavalent ($lysine_5$) cations lead to the formation of 3D bundles with hexagonal in-plane symmetry. (**Right**) Divalent cations [(Ba^{2+}, Ca^{2+}, Sr^{2+})] lead to the sheet-like 2D bundles with linear, branched, and loop morphologies. Reprinted with permission from [17]. Copyright 2004, National Academy of Sciences, U.S.A.

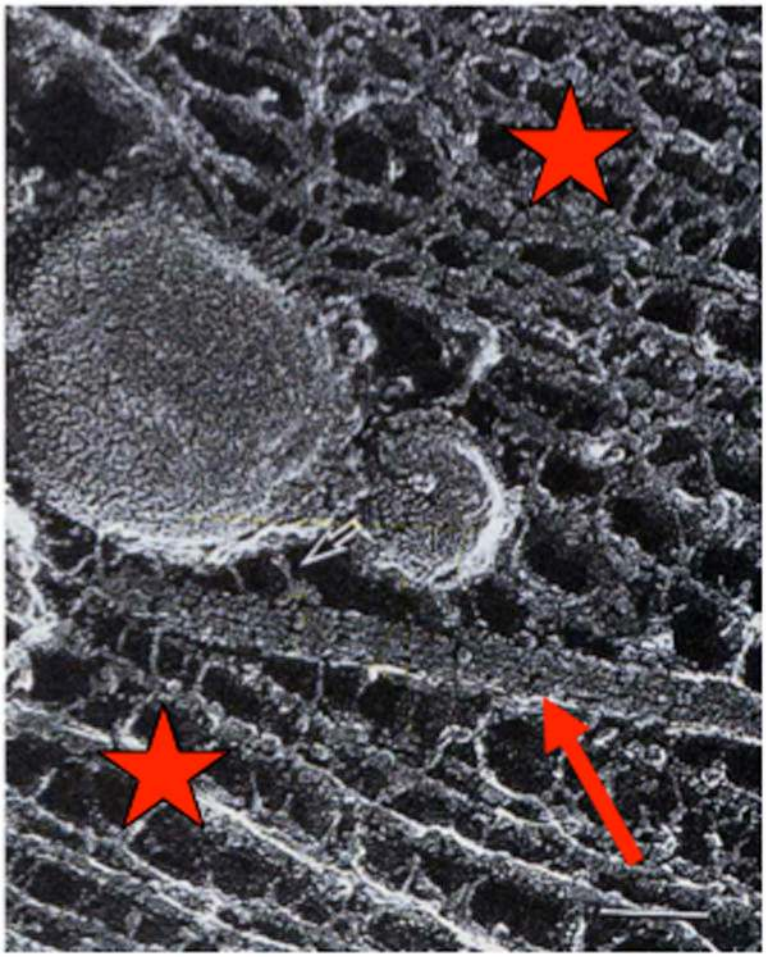

Figure 2.
Quick-frozen, deep-etched electron micrograph of a mouse nerve axon showing a microtubule (MT, red arrow) with an attached vesicle moving along the MT track via molecular motors. The MT is seen to be immersed in a network of Neurofilaments (NFs, red stars). The NF-networks in vertebrate axons form a nematic liquid crystal hydrogel. The scale in this micrograph can be seen by noting that the diameter of a MT is 25 nm. Reprinted from [7], with permission from Elsevier.

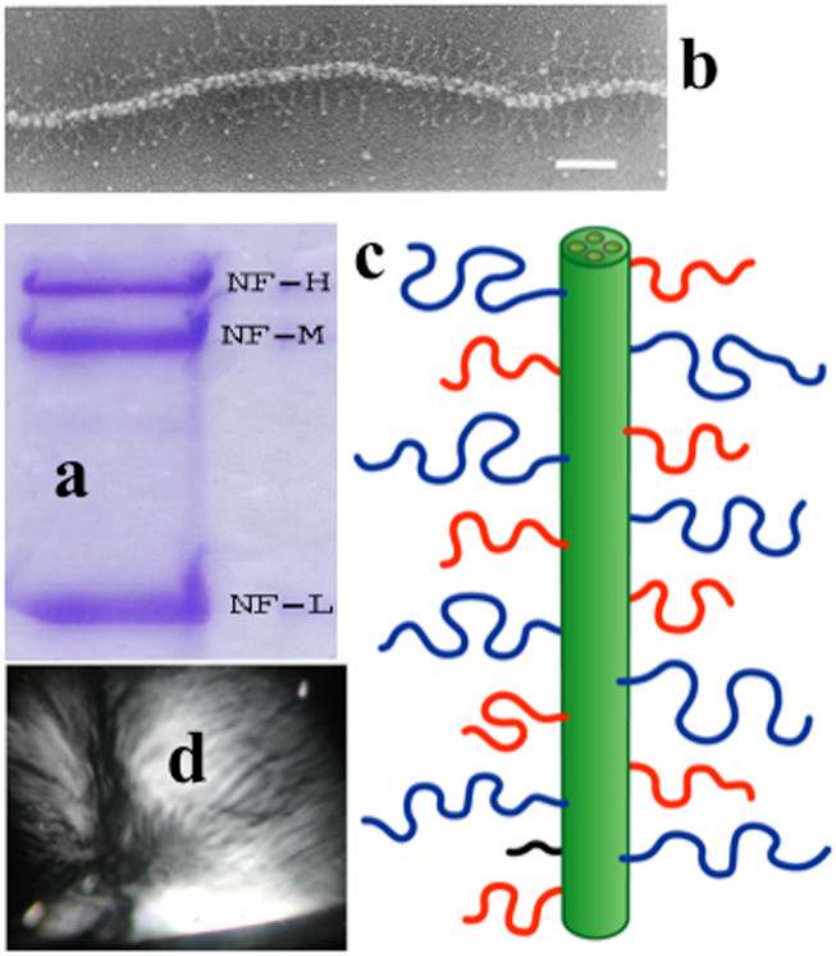

Figure 3.

(**a**) Gel electrophoresis (10% polyacrylamide in sodium dodecyl sulfate) of purified neurofilaments (NFs) showing the three subunits (NF-L, MW = 60K; NF-M, MW = 100K; NF-H, MW = 115K). NFs purified from bovine spinal cord according to the procedures described in [23, 25, 27]. (**b**) Electron micrograph of a mature neurofilament (glycerol sprayed/low-angle rotary metal shadowed on freshly cleaved mica). The sidearms are clearly visible. The bar is 100 nm. (**c**) Schematic of a NF showing the sidearms of NF-H (blue), NF-M (red), and NF-L (black) subunits containing 613, 514, and 158, amino acid residues respectively. (**d**) A reconstituted NF mixture forming a strongly birefringent hydrogel viewed between crossed polarizers shows the presence of nematic-like liquid crystalline texture. Parts a and d reprinted with permission from [22]; part b reprinted with permission from [6].

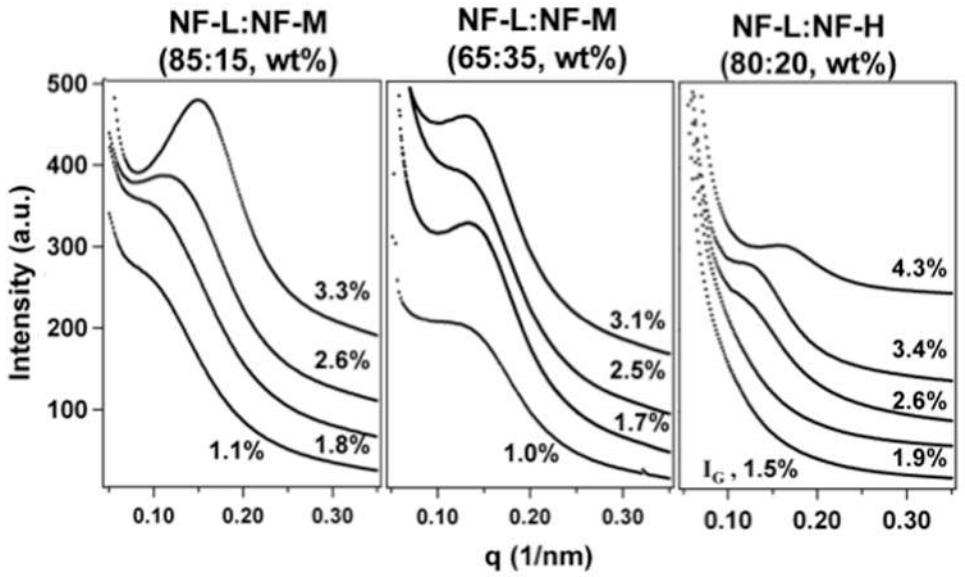

Figure 4.

Synchrotron SAXS data of NF-LM and NF-LH neurofilaments assembled from NF-L and NF-M (**Left** and **Middle**) and NF-L and NF-H (**Right**) subunits in 86 mM monovalent salt and pH ≈ 6.8. Each figure shows data along dilution lines (with decreasing total protein concentrations) for NF-L/NF-M = 85/15 (wt/wt), NF-L/NF-M = 65/35 (wt/wt) and NF-L/NF-H = 80/20 (wt/wt). Reprinted from [23], with permission from the Biophysical Society.

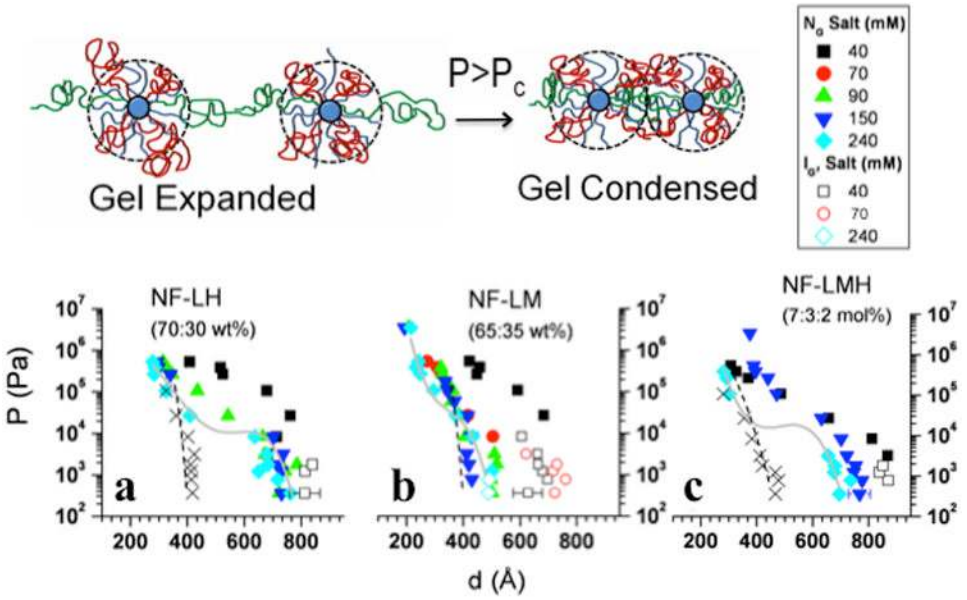

Figure 5.

(**Top**) End view of NF-LH, NF-LMH hydrogels undergoing a transition for $P > P_c$ from an expended-network to a condensed-network gel state with interpenetrating sidearm polyampholyte chains. (**Bottom**) Pressure-interfilament distance curves for NF hydrogels obtained using the SAXS-osmotic pressure technique. At ionic strengths 150 mM and 240 mM NF-LH (**a**) and NF-LMH (**c**) gels exhibit an expanded-network to condensed-network transition for $P > P_c \approx 10^4$ Pa, whereas NF-LM gels (**b**) are in a compressed state for $P < P_c$ and transition to the condensed state for $P > P_c$. (N_G = nematic gel; I_G = isotropic gel). At low ionic strengths (40 mM and 70 mM) NF-LM gels are expanded isotropic gels at $P < P_c$ and transition to the condensed-network state at $P > P_c$. Reprinted in part with permission from [25].

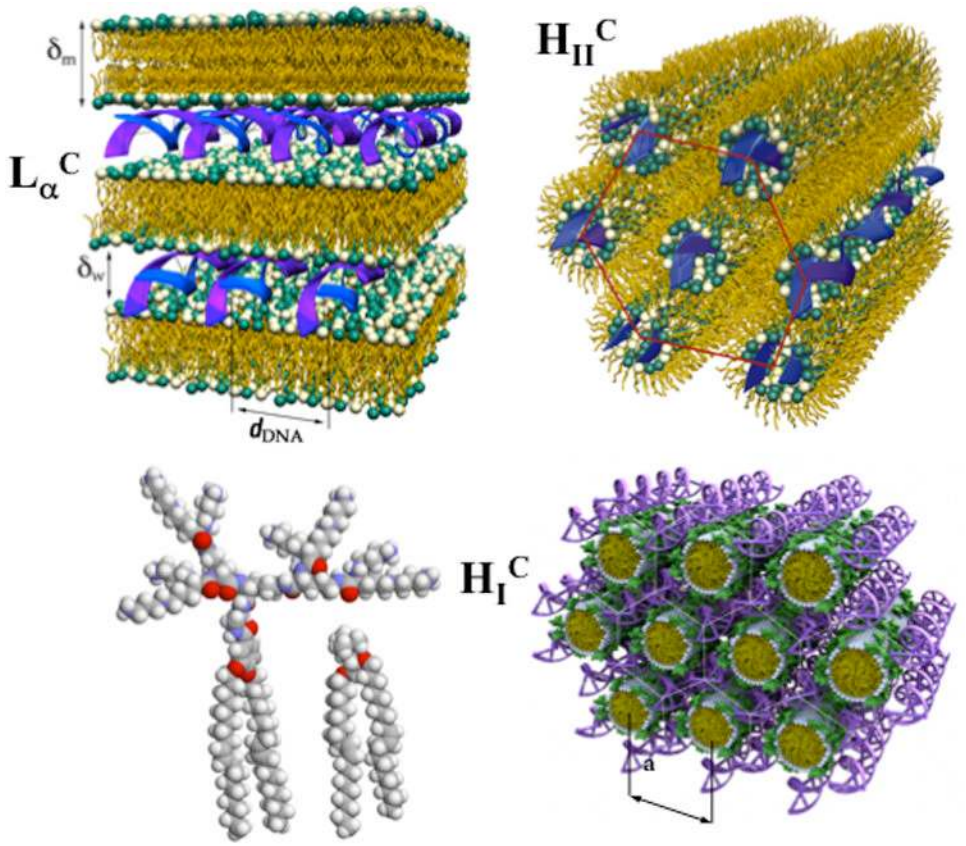

Figure 6.

The structure of three distinct cationic liposome (CL)-DNA complexes determined by synchrotron small-angle x-ray scattering. (**Top left**) The structure of the lamellar $L_\alpha{}^C$ phase of CL-DNA complexes with DNA sandwiched between lipid bilayers. The interlayer spacing is $d = \delta_w + \delta_m$. (**Top right**) The structure of the inverted hexagonal $H_{II}{}^C$ phase of CL-DNA complexes comprised of DNA coated with a lipid monolayer arranged on a hexagonal lattice. (**Bottom left**) Molecular models of hexadecavalent lipid MVLBG2 (16+) and monovalent lipid 1,2-dioleoyl-3-trimethylammonium-propane (DOTAP, 1+). (Bottom right) Schematic of the $H_I{}^C$ phase of CL-DNA complexes where the lipids consist of a mixture of MVLBG2 and 1,2-dioleoyl-*sn*-glycero-3-phosphocholine (DOPC). The large headgroup of MVLBG2 forces the lipid to assemble into cylindrical lipid micelles that are arranged on a hexagonal lattice. The DNA rods are arranged on a honeycomb lattice in the interstices of the lipid micelle arrangement. The interstitial space is filled by the headgroups, water and counterions. Interestingly, the DNA forms a three-dimensionally contiguous substructure in the $H_I{}^C$ phase, as opposed to isolated DNA rods and sheets of parallelly arranged strands in the $H_{II}{}^C$ and $L_\alpha{}^C$ phases, respectively. Bottom images reprinted with permission from [36]. Copyright 2006 American Chemical Society. Top images reprinted with permission from [35].

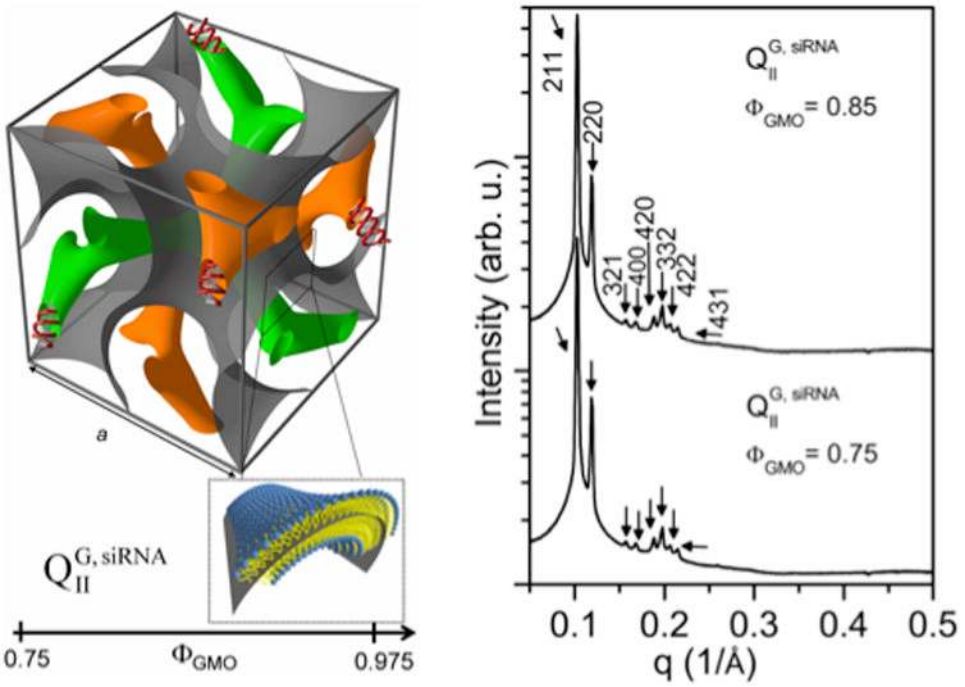

Figure 7.

(**Left**) The double gyroid lipid cubic phase incorporating functional short-interfering RNA (siRNA) within its two (green and orange) water channels. This phase, labeled $Q_{II}^{G,siRNA}$, is obtained for DOTAP/GMO-siRNA complexes with 1-monooleoyl-glycerol (GMO) molar fractions (Φ_{GMO}) of $0.75 \leq \Phi_{GMO} \leq 0.975$. A lipid bilayer surface separates the two intertwined but independent water channels. For clarity, the bilayer (which has a negative Gaussian curvature $C_1C_2 < 0$) is represented by a surface (grey) corresponding to a thin layer in the center of the membrane as indicated in the enlarged inset. (**Right**) Synchrotron small-angle X-ray scattering data for DOTAP/GMO in 30 wt% water containing siRNA molecules at $\Phi_{GMO} = 0.75$ (below) and at $\Phi_{GMO} = 0.85$ (above). The large number of reflections for the $Q_{II}^{G,siRNA}$ phase result from a body centered gyroid cubic structure with space group Ia3d. Reprinted with permission from [37]. Copyright 2010 American Chemical Society.